Tissue-specific extracellular matrix scaffolds for the regeneration of spatially complex musculoskeletal tissues

AUTHOR(S)

Grainne M. Cunniffe, Pedro J. Díaz-Payno, Eamon Sheehy, Susan E. Critchley, Henrique V. Almeida, Pierluca Pitacco, Simon F. Carroll, Olwyn R. Mahon, Aisling Dunne, Tanya J. Levingstone, Conor J. Moran, Robert Thomas Brady, Fergal O'Brien, Pieter A.J. Brama, Daniel J. Kelly

HANDLE

10779/rcsi.18742406.v1

URL

https://repository.rcsi.com/articles/journal_contribution/Tissue-specific_extracellular_matrix_scaffolds_for_the_regeneration_of_spatially_complex_musculoskeletal_tissues/18742406/1

Accepted Manuscript

Tissue-specific extracellular matrix scaffolds for the regeneration of spatially complex musculoskeletal tissues

Gráinne M. Cunniffe, Pedro J. Díaz-Payno, Eamon J. Sheehy, Susan E. Critchley, Henrique V. Almeida, Pierluca Pitacco, Simon F. Carroll, Olwyn R. Mahon, Aisling Dunne, Tanya J. Levingstone, Conor J. Moran, Robert T. Brady, Fergal J. O'Brien, Pieter A.J. Brama, Daniel J. Kelly

Please cite this article as: Cunniffe GráM, Díaz-Payno PJ, Sheehy EJ, Critchley SE, Almeida HV, Pitacco P, Carroll SF, Mahon OR, Dunne A, Levingstone TJ, Moran CJ, Brady RT, O'Brien FJ, Brama PAJ, Kelly DJ, Tissue-specific extracellular matrix scaffolds for the regeneration of spatially complex musculoskeletal tissues, *Biomaterials* (2018), doi: https://doi.org/10.1016/j.biomaterials.2018.09.044.

Tissue-specific extracellular matrix scaffolds for the regeneration of spatially complex musculoskeletal tissues

Gráinne M. Cunniffe [a, b, c, 1], Pedro J. Díaz-Payno [a, b, 1], Eamon J. Sheehy [a, b, d], Susan E. Critchley [a, b], Henrique V. Almeida [a, b], Pierluca Pitacco [a, b], Simon F. Carroll [a, b], Olwyn R. Mahon [a, b, e], Aisling Dunne [e], Tanya J. Levingstone [c, d], Conor J. Moran [c, d], Robert T. Brady [c, d], Fergal J. O'Brien [a, b, c, d], Pieter A.J. Brama [f], Daniel J. Kelly [a, b, c, d, *]

[a] Trinity Centre for Bioengineering, Trinity Biomedical Sciences Institute, Trinity College Dublin, Dublin, Ireland.
[b] Department of Mechanical and Manufacturing Engineering, School of Engineering, Trinity College Dublin, Dublin, Ireland.
[c] Advanced Materials and Bioengineering Research Centre (AMBER), Royal College of Surgeons in Ireland and Trinity College Dublin, Dublin, Ireland.
[d] Tissue Engineering Research Group, Department of Anatomy, Royal College of Surgeons in Ireland, Dublin, Ireland.
[e] Molecular Immunology Group, School of Biochemistry and Immunology, Trinity College Dublin, Dublin, Ireland.
[f] School of Veterinary Medicine, University College Dublin, Dublin, Ireland.

[1] These authors contributed equally.

* Corresponding author at: Department of Mechanical and Manufacturing Engineering, School of Engineering, Trinity College Dublin, Dublin 2, Ireland. Tel.: +353 1 896 3947; fax: +353 1 679 5554. E-mail address: kellyd9@tcd.ie

Keywords

Abstract

Biological scaffolds generated from tissue-derived extracellular matrix (ECM) are commonly used clinically for soft tissue regeneration. Such biomaterials can enhance tissue-specific differentiation of adult stem cells, suggesting that structuring different ECMs into multi-layered scaffolds can form the basis of new strategies for regenerating damaged interfacial tissues such as the osteochondral unit. In this study, mass spectrometry is used to demonstrate that growth plate (GP) and articular cartilage (AC) ECMs contain a unique array of

regulatory proteins that may be particularly suited to bone and cartilage repair respectively. Applying a novel iterative freeze-drying method, porous bi-phasic scaffolds composed of GP ECM overlaid by AC ECM are fabricated, which are capable of spatially directing stem cell differentiation *in vitro*, promoting the development of graded tissues transitioning from calcified cartilage to hyaline-like cartilage. Evaluating repair 12-months post-implantation into critically-sized caprine osteochondral defects reveals that these scaffolds promote regeneration in a manner distinct to commercial control-scaffolds. The GP layer supports endochondral bone formation, while the AC layer stimulates the formation of an overlying layer of hyaline cartilage with a collagen fiber architecture better recapitulating the native tissue. These findings support the use of a bi-layered, tissue-specific ECM derived scaffolds for regenerating spatially complex musculoskeletal tissues.

Graphical abstract
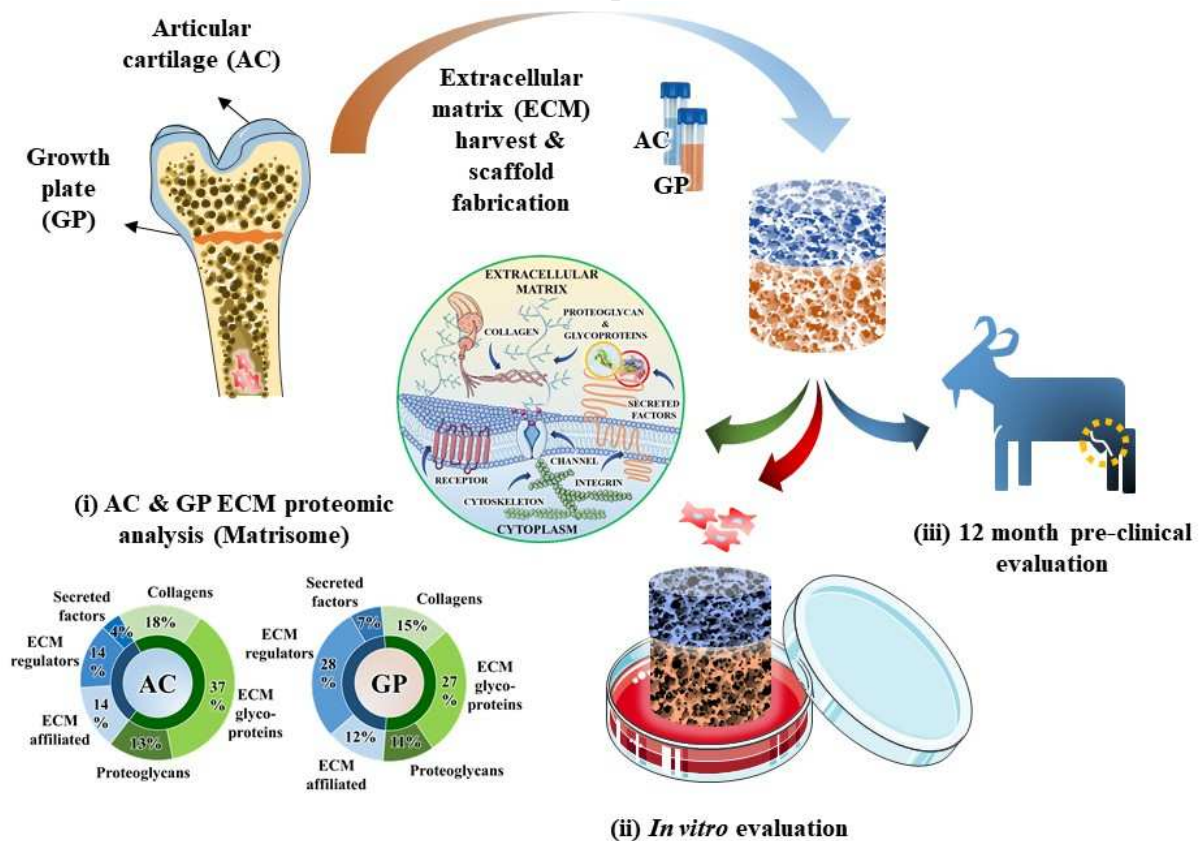
1. Introduction

Extracellular matrix (ECM) derived biomaterials have been used clinically over 1 million times in the surgical repair of different tissues and organs [1–5]. While the exact mechanism by which these bioactive scaffolds promote regeneration remains unclear, in the early stages of healing, the ECM supports the development of a pro-regenerative immune response involving both the adaptive and the innate immune system [6]. In particular, a favorable regenerative outcome has been linked to a ratio of M2 (anti-inflammatory) to M1 (pro-inflammatory) macrophages that facilitates tissue remodeling [7]. Scaffolds used clinically are typically derived from small intestine submucosa (SIS) or pericardium, and while the ECM of these tissues clearly contain structural and regulatory biomolecules generally supportive of regeneration [8], it is unlikely that a single tissue source of ECM will be optimal for all clinical targets. This concept is strengthened by recent studies reporting that ECM derived biomaterials can direct the differentiation of mesenchymal stem cells (MSCs) towards the phenotype of the source tissue from which they were derived [9–11]. This motivates the development of tissue-specific ECM derived scaffolds, potentially consisting of different layers or lineage-specific regions [12–14], especially when attempting to regenerate complex multi-phasic tissues such as the osteochondral unit of synovial joints. Articular cartilage possesses a poor regenerative capacity, with tissue damage typically progressing across the joint surface and into the underlying subchondral bone. If left untreated, these osteochondral defects can progress to osteoarthritis of the joint, motivating the need for new regenerative strategies to repair damaged synovial joints.

Cartilaginous tissues play key roles in the development and function of the musculoskeletal system. The epiphyseal plate or growth plate (GP), a cartilaginous tissue in the metaphysis at each end of a developing long bone, is responsible for its longitudinal growth through a

3

coordinated process of endochondral ossification (*the replacement of cartilage with bone*). Articular cartilage (AC), a form of hyaline cartilage, lines the ends of bones within synovial joints and functions to provide a smooth, low-friction surface for articulation and to facilitate the transmission of load across the joint. The ECM of both GP and AC have been successfully used to produce scaffolds for tissue engineering, with GP derived biomaterials shown to support large bone defect healing [15–17], and AC derived scaffolds shown to support chondrogenesis [9,18,19]. To better understand their regenerative potential, we first compared the proteome of solubilized GP and AC, demonstrating that they contain a unique array of regulatory factors potentially important to bone and cartilage regeneration. Furthermore, porous scaffolds derived from these two ECMs supported the development of distinct tissue types when seeded with MSCs. Based on these findings, we hypothesized that a bi-phasic scaffold consisting of spatially distinct but integrated layers of GP and AC ECM could be used to regenerate osteochondral defects. This study describes the capacity of these scaffolds to spatially direct MSC differentiation *in vitro* and the mechanism by which they can direct joint repair *in vivo* following their cell-free implantation in critically-sized caprine osteochondral defects.

2. Material and methods

2.1. Tissue harvest and scaffold fabrication

Articular cartilage (AC) and growth plate (GP) ECM tissues were harvested from porcine hind limbs (3-4 months old), purchased from a local abattoir shortly after sacrifice. The AC was obtained from the femoral head using a biopsy punch. Subsequently, the head of the bone was split open using a saw to reveal the epiphyseal line and to gain access to the GP, which was then carefully extracted using a scalpel. The AC and GP tissues were separately

pulverized using a cryomiller (SPEX SamplePrep®, NJ, USA), whereby liquid nitrogen was used to freeze the samples before mechanically grinding (3 x 1 min cycles) to create ECM powders. These powders were then re-suspended to form AC and GP slurries at 500 mg/ml in ddH$_2$O. Slurries were freeze-dried to generate AC and GP scaffolds for initial *in vitro* characterization, as previously described [9,20] (Φ5 x h3 mm). Briefly, the slurry temperature was reduced to −30 °C (1 °C/min) and maintained for 1 h to allow for ice-crystal nucleation and growth. The temperature was then increased to −10 °C (1 °C/min), followed by a hold of 24 h to allow for sublimation of the frozen water, and then finally increased to room temperature (0.5 °C/min). Scaffolds then underwent dehydrothermal crosslinking (DHT) in a vacuum oven (VD23, Binder, Germany), at 105 °C, at 0.5 mbar for 24 h. For the bi-layered scaffolds a novel, iterative freezing step was introduced. The GP slurry was firstly frozen within custom-made polydimethylsiloxane (PDMS) cylindrical molds to -20 ℃ (1°C/min) before an upper layer of AC slurry was added and subsequently frozen (AC-GP scaffolds prepared for *in vitro* analysis: Φ5 x h1.5 mm each layer, total height 3 mm; for *in vivo* evaluation AC layer: Φ6 x h2 mm and GP layer: Φ6 x h4 mm, total height 6 mm) before undergoing lyophilization and DHT as described above. Scaffolds were imaged using scanning electron microscopy (SEM) following fixation, alcohol dehydration and gold-palladium coating and pore size was calculated using Image J.

2.2. Protein analysis

ECM powders were treated with 6M Guanidine-hydrochloride for protein extraction [21]. Precipitation of soluble proteins was done using trichloroacetic (TCA) solution, acetone, 6 M urea in 50 mM ammonium bicarbonate (ABC) followed by treatment in 5 mM dithiothreitol (DTT) at 60 °C for 30 min, 10 mM iodoacetamide (IAA) at room temperature for 30 min and trypsin digestion prior to mass spectrometry analysis and western blot details. The samples were run on a Thermo Scientific Q Exactive mass spectrometer connected to a Dionex

Ultimate 3000 (RSLCnano) chromatography system. Tryptic peptides were resuspended in formic acid. Each sample was loaded onto a fused silica emitter (75 μm ID, pulled using a laser puller (Sutter Instruments P2000)), packed with UChrom C18 (1.8 μm) reverse phase media (nanoLCMS Solutions LCC) and was separated by an increasing acetonitrile gradient over 45/60 minutes at a flow rate of 250 nL/min. The mass spectrometer was operated in positive ion mode with a capillary temperature of 320 °C, and with a potential of 2300V applied to the frit. All data was acquired with the mass spectrometer operating in automatic data dependent switching mode. A high resolution (70,000) MS scan (300-1600 m/z) was performed using the Q Exactive to select the 8 most intense ions prior to MS/MS analysis using HCD. The raw data was *de novo* sequenced and searched against the *sus scrofa* complete Uniprot database using the search engine Maxquant [22–24], for peptides cleaved with trypsin. Each peptide used for protein identification met specific Maxquant parameters, i.e. only peptide scores that corresponded to a false discovery rate (FDR) of ≤1% were accepted. Proteins identified by Maxquant were processed with Perseus [25] in order to elucidate differences across the two tissues. MatrisomeDB [26] was used to cluster proteins into subgroups in order to find protein-protein interactions and to identify target molecules of interest.

2.3. In vitro analysis

Bone marrow derived mesenchymal stem cells (MSCs) were harvested following a standard protocol, from porcine hind limbs (3-4 months old), purchased from a local abattoir shortly after sacrifice. MSCs were used at passage 2 and seeded at a density of 500,000 cells per scaffold. Constructs were cultured in chondrogenic medium containing 10 ng/ml transforming growth factor β3 (TGF-β3, R&D Systems®). Cell viability was assessed at day 7 using live/dead staining (2 mM EthD-1 and 5 mM Calcein for 1 h) and confocal microscopy.

2.4. Histological and biochemical analysis

Samples at day 0 and day 28 (n=3) were fixed in 4% paraformaldehyde, dehydrated and wax embedded to allow serial slicing (6 μm) at the center of the constructs. Staining was performed using 1% alcian blue 8GX in 0.1 M HCl, picro-sirius red and alizarin red for evaluation of sGAG, collagen and calcium deposition, respectively. Collagen type II, X, I and VEGF synthesis was evaluated using a standard immunohistochemical technique with the appropriate primary antibody; 1:100 IgG mouse monoclonal anti-collagen type I (ab90395, Abcam®, UK), anti-collagen type II (ab3092, Abcam®, UK), 1:100 IgM mouse monoclonal anti-collagen type X (ab49945, Abcam®, UK) or 1:200 IgG rabbit polyclonal anti-VEGF (ab46154, Abcam®, UK). Biochemical analysis was also used to supplement histological findings by measuring sGAG (dimethylmethylene blue dye-binding assay from Blyscan, Biocolor Ltd, Northern Ireland), collagen (Chloramine-T assay, hydroxyproline:collagen ratio of 1:7.69 [27]) and calcium content (O-cresolphthalein complexone assay, Sentinel Diagnostics) in papain digested samples (n=3), as previously described [11].

2.5. In vivo implantation

Surgical procedure in caprine model was carried out as previously described [14]. Briefly, the goats were sedated using diazepam (0.3 – 0 .4 mg/kg IV) and butorphanol (0.2 mg/kg IV). An epidural was administered using morphine (0.2 mg/kg). Following placement of an intravenous catheter, anesthesia was induced with propofol (max. dose 4 mg/kg IV). Anesthesia was maintained using isoflurane with ventilation to maintain normal end tidal CO_2 between 4.6 and 6 kPa. Isotonic fluids were provided at 10 ml/kg/h. Following induction of anesthesia, the goats were placed in dorsal recumbency and an arthrotomy of each stifle joint was then performed using the lateral para-patellar approach. A critically-sized defect, 6 mm in diameter x 6 mm in depth, was created in each medial femoral condyle using a hand

drill, a flattened drill bit and a depth guide. The joint was flushed with normal fluids (0.9 % NaCl) and the stifle joints were assigned to one of the two treatment groups: 1) Maioregen scaffold (Finceramica), herein called the Control scaffold and 2) AC-GP ECM derived bi-layered scaffold, herein called the AC-GP scaffold. The commercial scaffold was cut to a diameter of 6 mm and to a depth of 6 mm in accordance with the manufacturers' guidelines. Both scaffold types were press fit into the defect site cell-free before routine closure of the joint capsule, subcutaneous tissues and skin. Morphine (0.1 - 0.2 mg/kg IM) and non-steroidal anti-inflammatory drugs (NSAIDs) [Carprofen (1.5 - 2.5 mg/kg subcutaneously) (Rimadyl)] were administered at the end of anesthesia. Following surgery, goats were housed in small indoor pens to allow skin incisions to heal and were allowed full weight bearing immediately. During this period the animals were closely monitored to ensure adequate analgesia. NSAIDs and antibiotics [Amoxicillin (Noroclav)] were administered for 5 days post-surgery. Two weeks post-operatively, following removal of sutures, animals were let out to pasture for the remainder of the study period. Euthanasia was carried out with an overdose of sodium pentobarbital (Euthatal) administered by I.V. injection at 6 and 12 month time points ($n \geq 6$) to permit harvesting of the treated condyles. Ethical evaluation and approval was administered by University College Dublin (AREC 12-71) and the Irish Government Department of Health (B100/4517).

2.6. Repair tissue evaluation

Macroscopic evaluation of the joints was performed immediately upon opening the joint (Table 1). 1.5 cm^3 sections containing the defect site were harvested, samples were fixed in a formalin solution and the levels of mineralization within the repair tissue (5 mm diameter cylindrical region) was quantified using μCT (Scanco Medical, Switzerland) at a threshold of 210, corresponding to a density of 399.5 mg hydroxyapatite/cm^3. Demineralized wax-embedded constructs were sectioned at 10 μm and stained with safranin O, hematoxylin and

8

eosin and picro-sirius red and immunostained for collagen type II for ICRS evaluation (Fig. S3 and Table S1) [28]. Safranin O staining was also used in combination with Photoshop CS6 to quantify the area of positively stained cartilage within a region of interest (ROI) in the articular cartilage and subchondral bone regions of the repair tissue. Picro-sirius red stained samples were imaged under polarized light microscopy to investigate collagen fiber orientation. Directionality plugin [29] from Image J was used to quantify the mean orientation and angular dispersion of the collagen fibers observed in the superficial and deep zones of the regenerated articular cartilage (Fig. S4).

Table 1. Macroscopic scoring system for cartilage repair. Maximum score possible is 12.

Characteristic	Grading	Score
Degree of defect repair	In level with surrounding cartilage	4
	75 % repair of defect depth	3
	50 % repair of defect depth	2
	25 % repair of defect depth	1
	0 % repair of defect depth	0
Integration to border zone	Complete integration with surrounding cartilage	4
	Demarcating border < 1 mm	3
	¾ implant integrated with surrounding cartilage, ¼ notable border > 1 mm	2
	½ implant integrated with surrounding cartilage, ½ notable border > 1 mm	1
	From ¼ implant integrated to no contact with surrounding cartilage	0
Macroscopic appearance	Intact smooth surface	4
	Fibrillated surface	3
	Small, scattered fissures or cracks	2
	Several, small or few but large fissures	1
	Total degeneration of grafted area	0

2.7. Statistical analysis

All statistical analyses were performed using GraphPad Prism, except for mass spectrometry which was analyzed using Perseus. All values are reported as means ± standard deviation. Significance for all statistical analyses was defined as $p < 0.05$.

3. Results

3.1. Growth plate and articular cartilage contain shared and distinct regulatory proteins

Growth plate (GP) and articular cartilage (AC) ECM from the femur of skeletally immature pigs (Fig. 1a) were found to contain a range of shared and distinct proteins (Table S1 and Table S2). Of the 297 proteins identified within AC, 89% of these were also detected within GP, however, of the 603 proteins detected in the GP tissue, the majority (56%) were not found in AC (Fig. 1b and c). Further bioinformatics analysis and filtering, through MatrisomeDB [26], revealed that the two tissues contained a similar number of core matrisome proteins, including collagens, ECM glycoproteins and proteoglycans (Fig. 1d). The GP tissue, however, contained more abundant matrisome-associated proteins such as ECM-affiliated, ECM regulators, and secreted factors. Of interest was the finding that the GP contained proteins that are believed to play a role in angiogenesis, such as CSPG4 [30,31] and ANGPTL2 [32,33]; and osteogenesis, including CLEC11A [34], MMP13 [35,36] and S100A10 [37,38]. In contrast, AC contained factors known to inhibit hypertrophy and to promote chondrogenesis, such as GREM1, FRZB [39] and TGFβi [40,41]. The differential presence of selected key proteins detected using mass spectrometry were also verified using western blots (Fig. 1e).
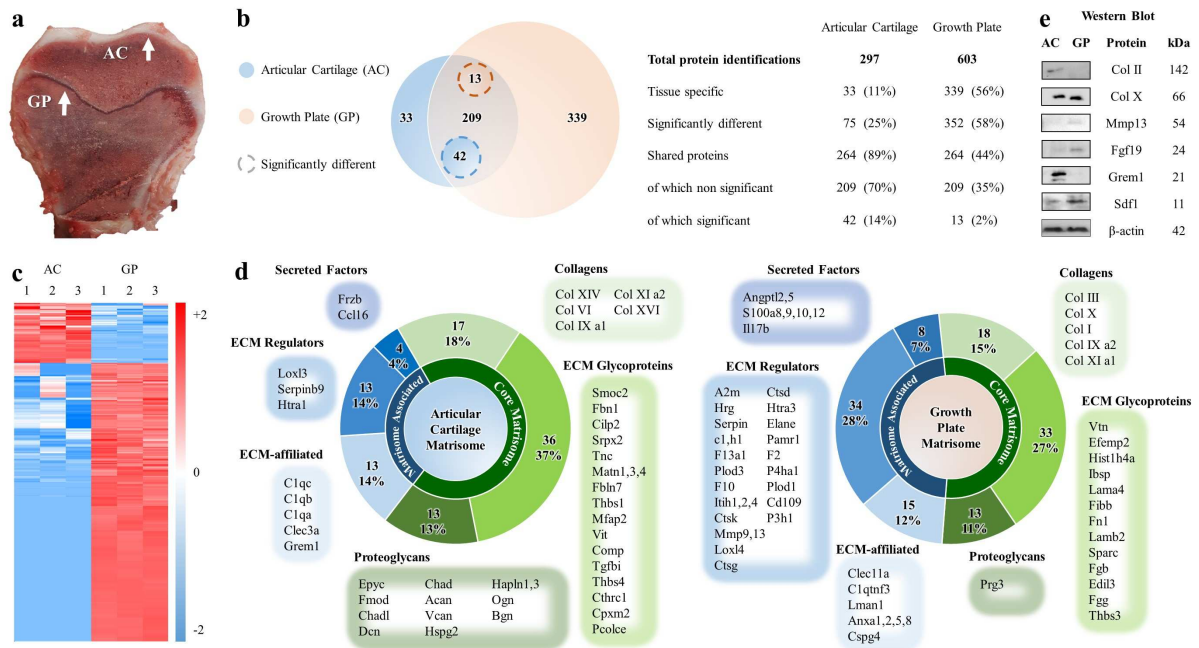
10

Fig. 1. Comparison of Articular Cartilage (AC) and Growth Plate (GP) ECM proteome. a) Macroscopic image demonstrating the location of the harvested AC and GP ECM within a porcine femur. b) Venn diagram of the total numbers of proteins identified via mass spectrometry which were either specific to, or shared by AC or GP tissues. c) Heat map of the mass spectrometry analysis of soluble factors present within 3 biological replicates of AC and GP tissues. d) Characterization of the total number of proteins detected in each tissue, categorized into core matrisome or matrisome-associated proteins. The listed proteins are the significantly expressed proteins identified in either AC or GP matrisomes, grouped into clusters associated with their structure and function. e) Western blot analysis of key proteins differentially detected in either tissue type.

3.2. AC and GP ECM derived scaffolds promote tissue-specific differentiation of MSCs

Having demonstrated that AC and GP contain distinct protein profiles, we next sought to verify that scaffolds produced using these two ECMs would provide tissue-specific cues to

11

encapsulated stem cells. Porous scaffolds were fabricated via freeze-drying of a suspension of either AC or GP derived ECM [9,20]. The scaffolds were found to facilitate the infiltration of bone marrow derived MSCs within 24 hours of seeding (Fig. 2a). Pores ranging in size from 10 to 300 μm, with a mean pore size of 109 ± 50 μm for AC and 126 ± 52 μm in GP scaffolds, were observed using SEM (Fig. S1). AC and GP scaffolds seeded with MSCs were then cultured under identical conditions for 28 days in the presence of transforming growth factor (TGF)-β3, with the resultant tissue deposition analyzed to evaluate the osteo- or chondro-inductive properties of the two different scaffolds. While both scaffolds supported the development of a cartilaginous tissue, significantly higher levels of sulphated glycosaminoglycan (sGAG) and collagen were deposited in the AC scaffolds (Fig. 2b and c), suggesting that this biomaterial was more supportive of hyaline cartilage development. In contrast, significantly higher levels of calcium deposition were detected within the GP scaffolds, suggesting that this biomaterial was more osteogenic and supported the development of a calcified cartilage. These apparent phenotypic differences were confirmed by immunohistochemical analysis which demonstrated enhanced deposition of collagen type X, collagen type I and vascular endothelial growth factor (VEGF) within the GP scaffolds, while higher levels of collagen type II deposition were observed within the AC scaffold (Fig. 2d). Taken together, these findings suggest that the GP ECM scaffolds support the development of a VEGF expressing calcified cartilage, while AC ECM derived scaffolds support the development of a hyaline-like cartilage rich in proteoglycans and collagen type II.
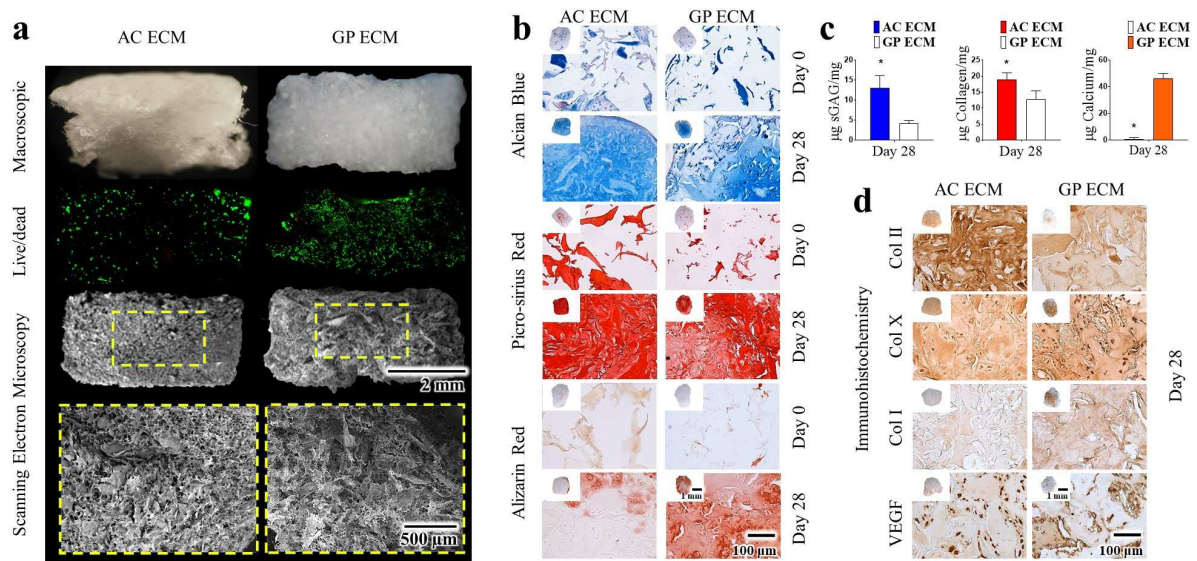
Fig. 2. ECM scaffolds regulate MSC differentiation *in vitro*. a) Macroscopic images of porous, freeze-dried scaffolds formed from either AC or GP ECM; confocal images stained for live/dead analysis of the distribution of MSCs throughout both scaffolds 24 h post-seeding; and SEM images of the scaffolds showing the interconnected pore structure achieved via controlled freeze-drying. b) Histological staining for sulphated glycosaminoglycan (sGAG), collagen and calcium deposition at day 0 and after 28 days in chondrogenic culture conditions. c) Quantification of sGAG, collagen and calcium deposition in each scaffold after 28 days. d) Immunohistochemical staining for collagen type II, collagen type X, collagen type I and VEGF; [*]p < 0.05, ANOVA.

3.3. Bi-layered ECM scaffolds facilitate the development of spatially complex tissues

Using a novel iterative freeze-drying process, AC and GP ECM were next combined to create a bi-layered porous scaffold with distinct but interconnected AC and GP regions (termed 'AC-GP scaffolds'; Fig. 3a). To investigate if these bi-layered AC-GP scaffolds could

13

spatially direct stem cell differentiation based solely on their differential composition, they were seeded with a single population of MSCs and cultured for 28 days in the presence of TGF-β3. Qualitative and quantitative evaluation of each ECM layer indicated that they were capable of driving tissue-specific stem cell differentiation and matrix deposition, with higher levels of sGAG and collagen deposition observed in the AC layer and higher levels of cartilage matrix calcification observed in the GP layer (Fig. 3b and c). More intense staining for collagen type II was observed within the AC layer of the scaffold, while higher levels of collagen type I and collagen type X accumulated within the GP layer. MSC-mediated deposition of VEGF was also higher in the GP layer of the scaffold (Fig. 3d). Together this data demonstrates that bi-layered AC-GP scaffolds are capable of spatially regulating the differentiation of MSCs to produce a graded tissue that transitions from calcified cartilage to hyaline cartilage.

Successful integration of ECM scaffolds within a defect site is also dependent on eliciting appropriate host immune responses; therefore, before commencing large animal studies preliminary assays were carried out to examine the effect of the different ECMs on the phenotype and secretome of primary human macrophages. It was observed that both ECM scaffolds evoked minimal IL-6, 10 and 12 production. Interestingly, GP ECM scaffolds induced the expression of higher levels of the chemokine IL-8 (Fig. S2), which has previously been shown to promote osteoclastogenesis [42,43]. AC scaffolds enhanced the mRNA expression of basic fibroblast growth factor (bFGF), a growth factor known to enhance chondrogenesis [44], while GP scaffolds enhanced the expression of pro-angiogenic factors VEGF and Angiopoietin 1 (ANG1).
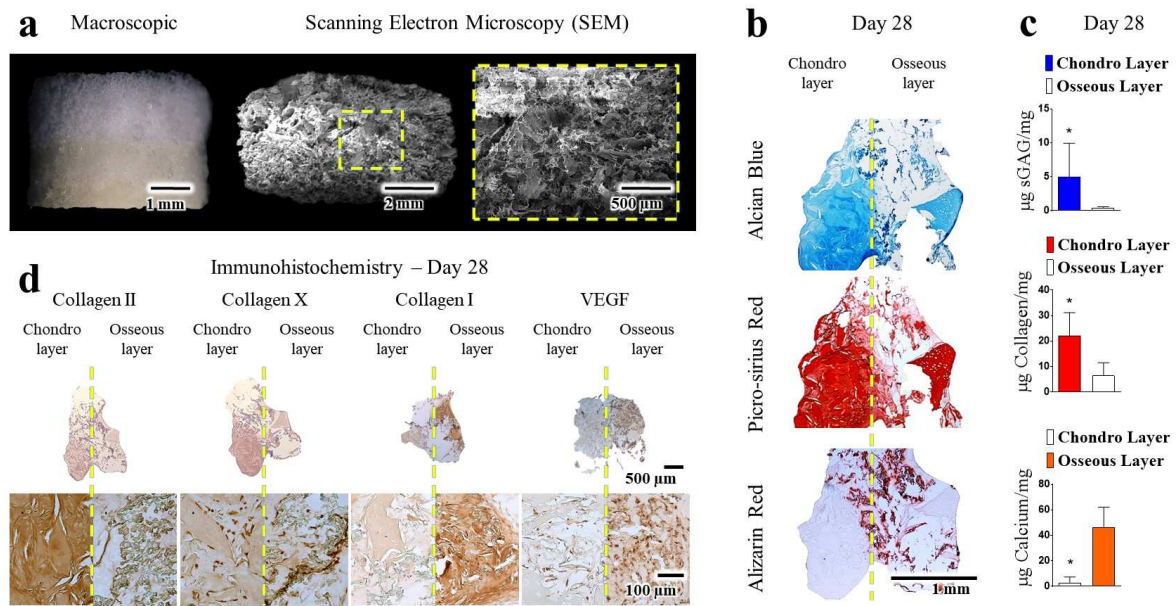
Fig. 3. Bi-layered ECM scaffolds spatially direct MSC differentiation *in vitro*. a) Macroscopic and SEM images of bi-layered AC-GP scaffolds demonstrating the spatial control, seamless interface and the inherent porosity achieved through the iterative freeze-drying procedure. b) Histological images of bi-layered scaffolds seeded with a single population of MSCs and evaluated for the deposition of sGAG, collagen and calcium after 28 days in chondrogenic culture conditions. c) Corresponding quantification of the sGAG, collagen and calcium deposition within each individual layer of the scaffold. d) Immunohistochemical staining for collagen type II, collagen type X, collagen type I and VEGF. *p < 0.05, ANOVA.

3.4. Bi-layered ECM derived scaffolds promote host-mediated osteochondral defect regeneration

To evaluate their regenerative potential *in vivo*, bi-layered AC-GP scaffolds were implanted (cell-free) into critically-sized osteochondral defects created in the medial femoral condyles of goats. 6 and 12 months after scaffold implantation, the quality of repair was compared to

15

that produced by implanting a collagen type I-based control scaffold (MaioRegen, Finceramica), which is currently in human clinical use for osteochondral defect repair [45]. The macroscopic appearance of defects treated with the two scaffolds appeared similar at both time-points (Fig. 4a), with no significant difference in the macroscopic score between the AC-GP scaffold and the control scaffold (Fig. 4a, b). Reconstructing images obtained from μCT scanning of the harvested osteochondral sections also demonstrated good regeneration of the bony region of the osteochondral defects treated with either scaffold (Fig. 4c). The bone volume within the subarticular spongiosa region of the defect (SAS; defined as the bottom 3 mm of the bony region of the defect) significantly increased between 6 and 12 months in defects treated with the AC-GP scaffolds, but not with the control scaffold (Fig. 4d). Bone volume in the subchondral bone plate (SBP; defined as the upper 1 mm of the bony region of the defect) was higher than in the subarticular spongiosa, however no significant differences in bone levels were observed between the two scaffolds in this region of the defect. Native bone has a similar bone volume value to the regenerated defects at 12 months (data not shown).
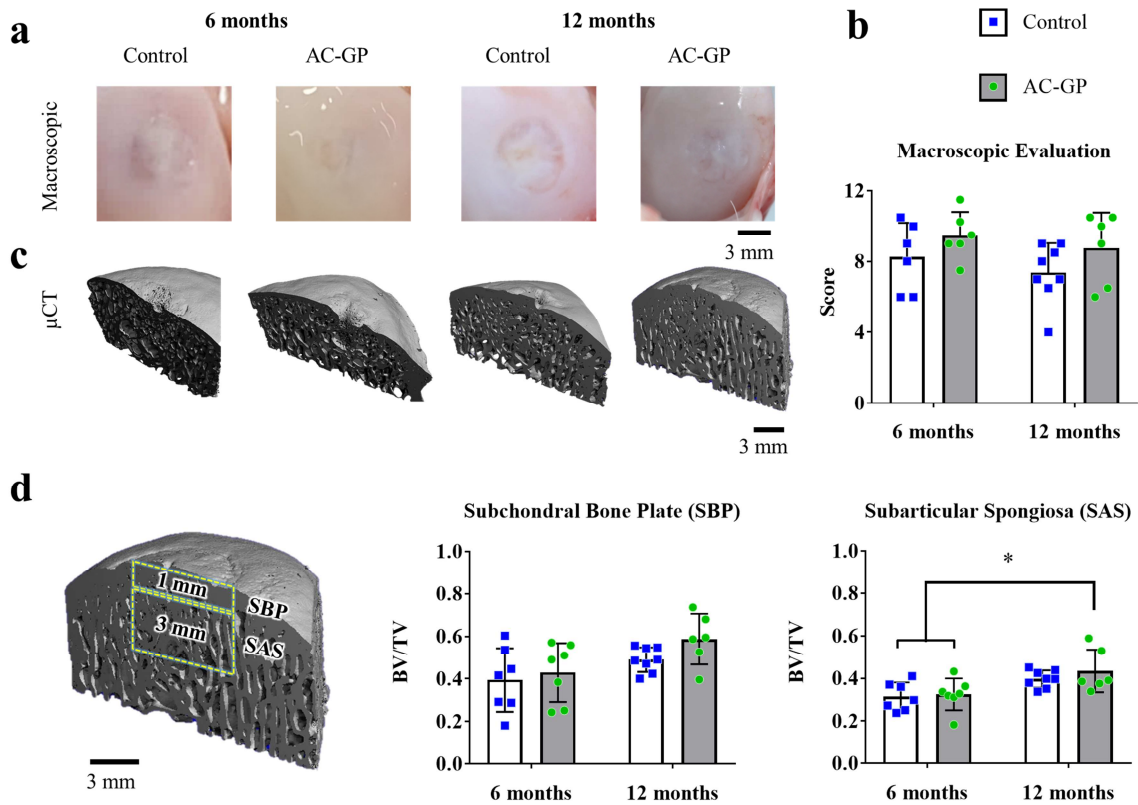
16

Fig. 4. Macroscopic and bone density analysis of healing within treated caprine osteochondral defects. a) Macroscopic representative images of healing achieved through the treatment of osteochondral defects with control scaffolds or bi-layered AC-GP scaffolds after 6 and 12 months, respectively, and b) quantification of the macroscopic appearance of the defects based on repair tissue integration, % defect fill and chondrogenic appearance. c) Reconstructed µCT images demonstrating the distribution of mineralized tissue across the center of the repair tissue at both time points. d) Quantification of the bone volume per total volume within two regions of the defect, the upper 1 mm subchondral bone plate region and the lower 3 mm subarticular spongiosa region at both time points. *$p < 0.05$, ANOVA.

Examining the repair tissue in more detail using standard histological techniques revealed that the percentage of repair tissue staining positive with safranin-O for proteoglycans (Fig.

5a), an indicator of cartilage tissue development, was significantly higher in the chondral regions of defects treated with the AC-GP scaffolds after 6 months (Fig. 5b). No significant difference was observed by 12 months (Fig. 5b). A trend towards higher levels of cartilage tissue formation within the subchondral region was observed in defects treated with the AC-GP scaffolds after 6 months, although this was not statistically significant. Cartilage levels within the osseous region of defects treated with the AC-GP scaffolds noticeably decreased between 6 and 12 months, suggesting that regeneration of the osseous region of the defect is occurring, at least in part, by endochondral ossification. The cartilage region of the repair tissue in both groups also stained positive for collagen type II, the predominant type of collagen found in hyaline cartilage (Fig. 5c). By 12 months, a collagen network organization similar to native condyles was detected more consistently in the AC-GP treated defects. The International Cartilage Repair Society (ICRS) scores [28] of these histological sections are provided in Fig. S3, with a trend towards higher "Average Cartilage" scores for the ECM treated group at both time points (6 months: Control 42.32 *vs.* AC-GP 54.52, 12 months: Control 51.14 *vs.* AC-GP 63.26).
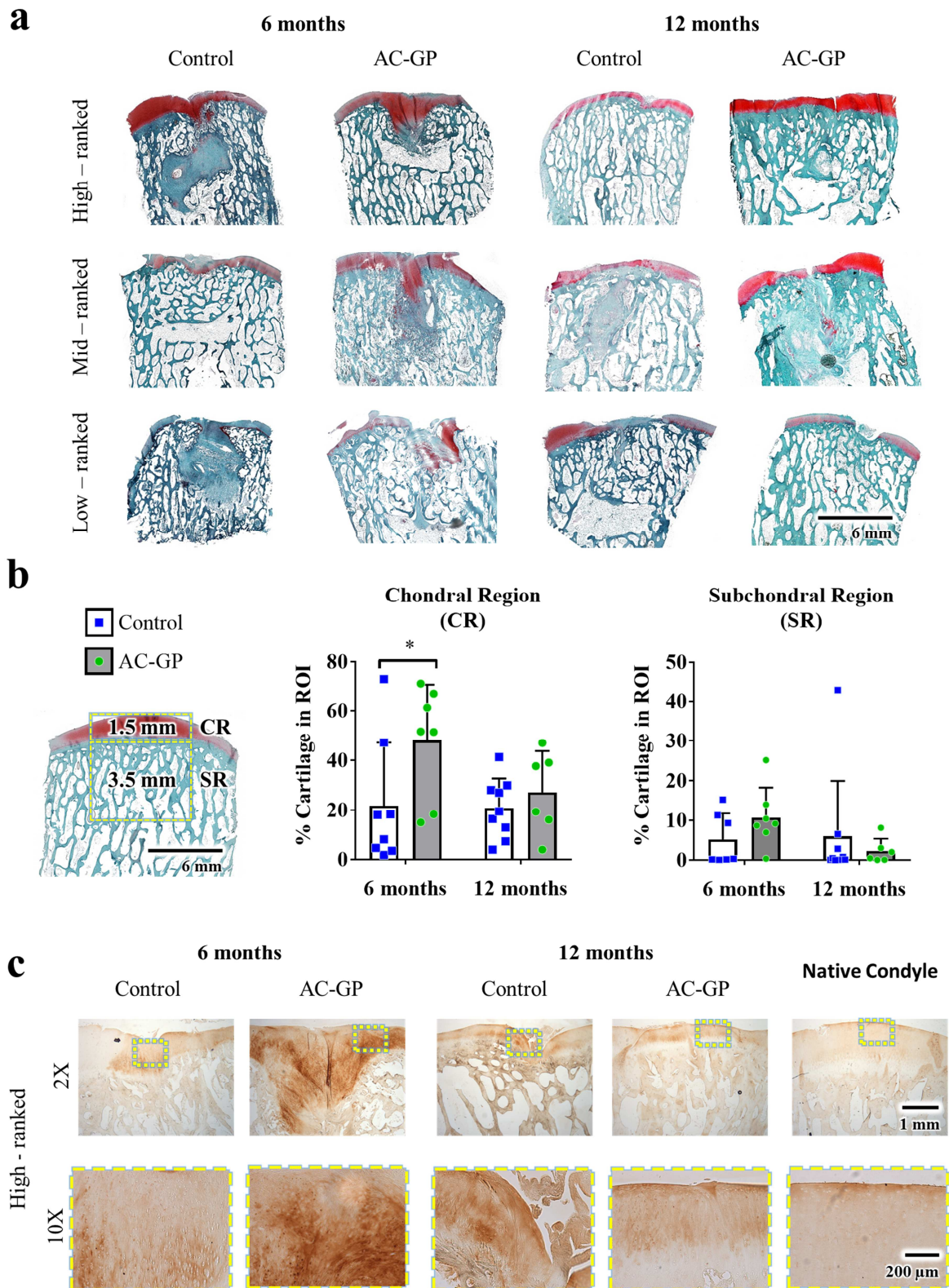
Fig. 5. Analysis of articular cartilage and subchondral bone repair following scaffold implantation. a) Cartilage matrix staining (red, safranin-O) for the highest-, mid- and lowest-

ranked samples at 6 and 12 months, scored blindly using established ICRS scoring methods (Fig. S3 and Table S1). b) Quantification of the percentage of tissue classified as cartilage in the upper chondral region, and in the lower subchondral region of the repair tissue at both time points. c) Collagen type II stained samples for control and AC-GP scaffold treated groups at 2x and 10x magnifications, shown next to a native condyle control. *p < 0.05, ANOVA.

Motivated by the histological findings which suggested the development of a more hyaline-like repair tissue in AC-GP scaffold treated defects, the organization of the newly formed collagen fiber network was examined in more detail using polarized light microscopy (PLM) (Fig. 6a), and the predominant angle of orientation and the dispersion of the fiber orientations were quantified in the upper (Top) superficial region, and deep (Bottom) cartilage region (Fig. 6 b and c), using *Directionality* plugin from Image J [29]. At both 6 and 12 months, the collagen fiber organization of the repair tissue within AC-GP treated defects was consistently more similar to native cartilage samples than the control group. A parallel fiber orientation (approaching 0 degrees) with a lower range of dispersion was observed at both time points in the superficial cartilage region of the AC-GP treated defects, while a perpendicular fiber orientation (approaching 90 degrees) was achieved more consistently in the deeper cartilage regions following treatment with the AC-GP scaffold.
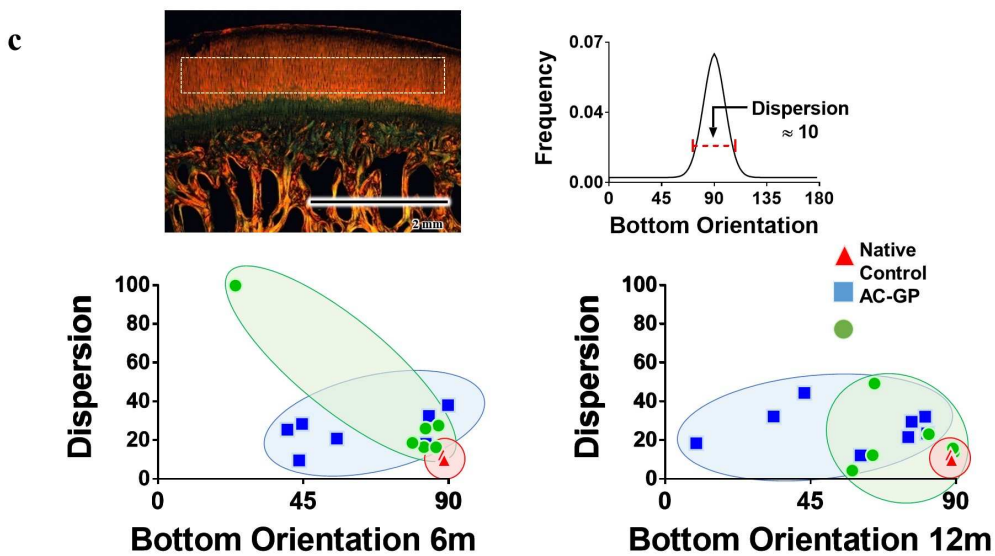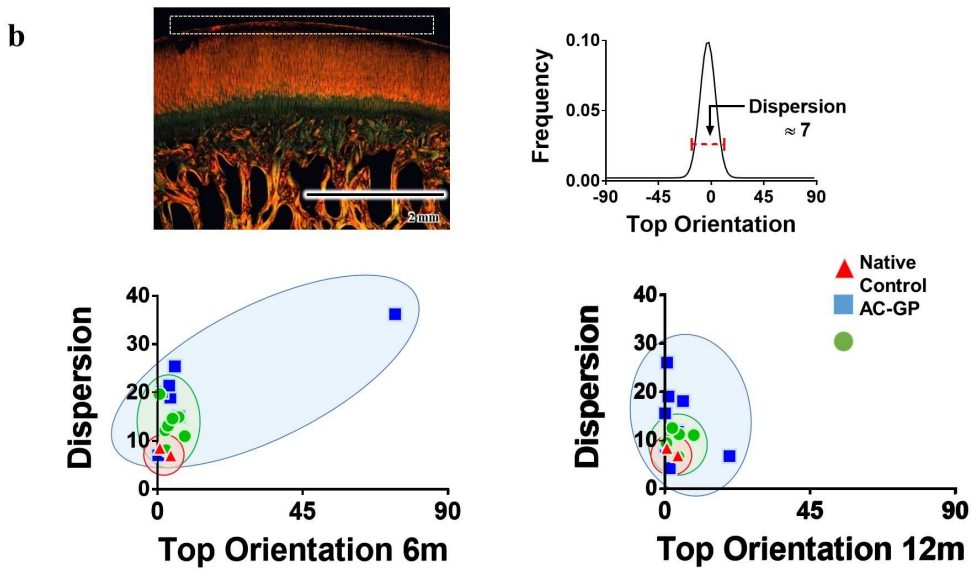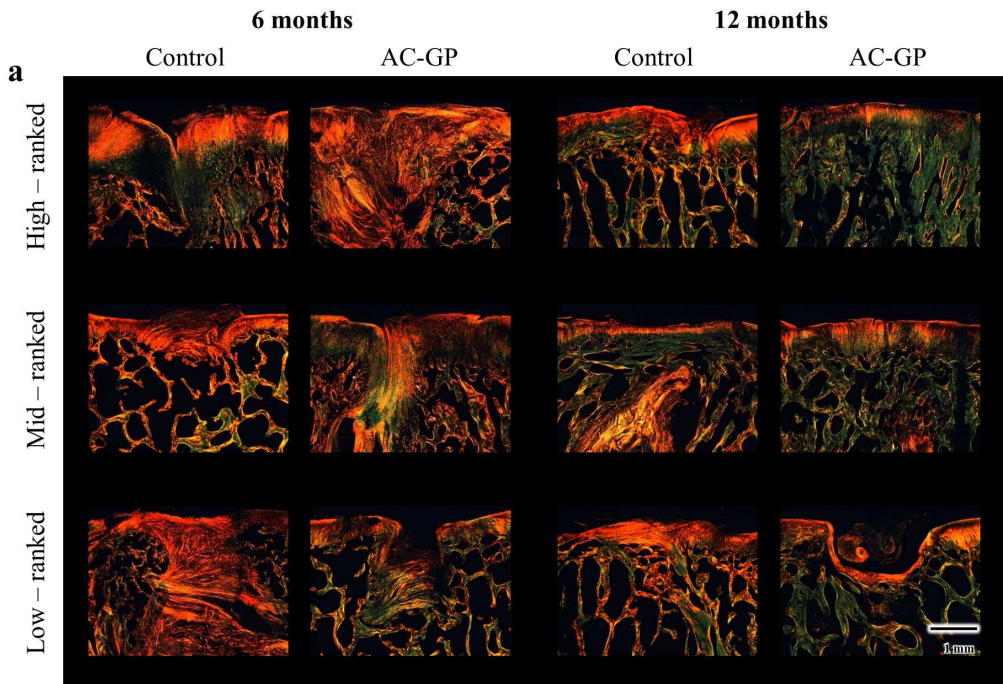
Fig. 6. Analysis of collagen fiber organization within repaired cartilage. a) PLM images indicating the orientation of the collagen fibers within the repair tissue of control and AC-GP scaffold treated groups at 6 and 12 months. b) Evaluation of the collagen fiber orientation in the superficial (Top) zone and c) deep cartilage (Bottom) zone within the repair tissue relative to a native condyle control at 6 and 12 months. A lower dispersion value indicates a more consistent fiber orientation within the sample. Fibers running parallel to the surface possess an orientation of 0 degrees, while fibers running perpendicular have an orientation of 90 degrees in native articular cartilage tissue.

4. Discussion

The results of this study demonstrate that bi-layered ECM derived scaffolds can direct tissue-specific stem cell differentiation *in vitro* and during regeneration of caprine osteochondral defects. In isolation, GP ECM derived scaffolds supported the development of a calcified cartilage tissue *in vitro,* confirming their potential for endochondral bone regeneration [11]. In contrast, the AC ECM derived scaffolds supported the development of an articular cartilage-like tissue that appeared more resistant to hypertrophy and endochondral ossification. These two ECMs were then combined using a novel freeze-drying technique to produce a bi-layered scaffold, which was found capable of spatially directing the differentiation of single population of MSCs *in vitro*, resulting in the development of a graded tissue that transitioned from calcified cartilage to hyaline-like cartilage. Over 12 months *in vivo*, these bi-layered ECM derived scaffolds promoted a distinct pattern of repair within caprine osteochondral defects, resulting in the regeneration of hyaline cartilage with a collagen fiber architecture that better recapitulated the native tissue compared to commercially available control scaffolds.

In vitro, we found that the different ECM derived scaffolds promoted the development of either calcified or hyaline cartilage following seeding with bone marrow derived MSCs. This can be correlated to the unique composition of each ECM, which was determined based on an in-depth analysis of the less abundant non-collagenous proteins in this tissue. The proteins detected in the GP using mass spectrometry analysis are in agreement with previous studies, confirming that hypertrophic chondrocytes resident in the GP express a number of angiogenic factors, including CSPG4 [30,46], ANGPT2 [32,47] and MMPs [48,49]; as well as osteogenic factors such as S100A10 [37,50], osteolectin (CLEC11A) [34], together with BMP [51] and FGF related proteins [52,53]. In addition, the GP will contain some mineralized cartilage, and residual mineral within the GP ECM derived scaffolds may also contribute to its osteo-inductivity [11]. In contrast to the GP, AC ECM derived scaffolds supported the development of a hyaline-like cartilaginous tissue. This can be attributed to the fact that the AC ECM is rich in type II collagen, which is known to be chondro-inductive [54], and the presence of hypertrophic inhibitors and cartilage homeostasis regulators such as GREM1 [39,55] and TGFβi/βIGH3 [40,41]. For instance, GREM1 is a highly conserved glycoprotein known to function as a BMP antagonist. GREM1 predominantly regulates BMP2, 4 and 7, and plays an essential role in normal progression of limb bud patterning development [55,56]. TGFβi is a protein induced by TGFβ and is believed to have an effect in the early stages of cartilage development by promoting the adhesion and growth of pre-chondrogenic cells, but negatively regulates mineralization during the terminal stages of chondrogenic differentiation [57]. Previous mass spectrometry studies of AC have also revealed the presence of these proteins at different depths in human articular cartilage and other cartilaginous tissues [58,59]. Our work builds on these previous studies, and when combined with the detailed mass spectrometry analysis of other tissue specific ECMs [26,60], provides an understanding for how the unique composition of GP and

23

AC might make them particularly suitable as base biomaterials for bone and articular cartilage repair, respectively.

Following a detailed analysis demonstrating the capacity of these bi-layered ECM derived scaffolds to support spatially defined stem cell differentiation *in vitro,* they were next compared to a market-leading scaffold (Maioregen) [61] for their capacity to promote osteochondral defect regeneration *in vivo*. This nano-composite multi-layered biomaterial has previously been shown to promote improved osteochondral defect regeneration compared to empty controls [62]. Healing of the osseous region of the OC defects appeared to occur via different mechanisms when comparing the control scaffold and experimental AC-GP ECM scaffolds. Following implantation of the AC-GP ECM derived scaffold, evidence of remnant cartilage tissue within the osseous phase of the defect was detected at 6 months, which appeared to be replaced by fully-integrated, mature bone at month 12. This suggests that bone regeneration was occurring, at least in part, by endochondral ossification. In contrast, the control scaffold appeared to elicit bone regeneration primarily via the intramembranous pathway, as minimal intermediary cartilage tissue was detected within the osseous region at either time point. This may be due to the composition of the control scaffold, specifically the magnesium enriched hydroxyapatite (Mg-HA) and collagen type I, which have been shown to induce direct ossification [63]. Interestingly, implantation of either scaffold resulted in similar levels of bone healing by 12 months. Development of such a well-integrated, stable subchondral bone plate is thought to be vital to facilitate and maintain an upper layer of healthy repair cartilage.

Six months after implantation, higher levels of cartilage tissue were detected in the chondral region of defects treated with the experimental ECM scaffold. Furthermore, the collagen network within the repair cartilage that formed following implantation of AC-GP scaffolds better mimicked the zonal architecture characteristic of native articular cartilage.

24

Development of an organized collagen fiber network is critical to support normal load bearing and extend the protective function of cartilage [64], potentially leading to superior long-term outcomes compared to that achieved when a more disorganized, fibro-cartilage repair tissue forms. It is tempting to speculate that the development of such an organized cartilage repair tissue is, at least in part, related to the underlying bone regenerating via endochondral ossification. During normal joint development, the cartilage functions as a surface growth plate prior to skeletal maturity [65], with zonally organized articular cartilage only emerging at skeletal maturity [64]. Therefore, the AC-GP scaffolds may be recapitulating aspects of normal joint development by promoting articular cartilage formation over a layer of transient cartilage that is undergoing endochondral ossification.

Porcine ECM is commonly used in the development of scaffolds used clinically for soft tissue repair, however, successful clinical translation of xenogeneic tissue-derived ECM scaffolds requires efficient decellularization of the tissue to prevent an adverse immune response [66]. While the AC-GP scaffolds did not appear to elicit any negative immune response *in vitro* or *in vivo*, further studies will be required to validate this prior to clinical translation in human. Furthermore, if more extensive decellularization protocols are deemed necessary, further mass spectrometry analysis will be required to establish how such chemical treatments influence the composition of the resulting scaffold. Additionally, comparative analysis to the composition of other ECM derived bioscaffolds (e.g. small intestinal submucosa) is warranted to further support the need for tissue-specific ECM derived scaffolds for the regeneration of complex tissues. There are some other limitations with the proposed strategy for joint regeneration. While both scaffolds promoted hyaline cartilage tissue formation, it should be noted that this was not consistently attained in either group, with some animal-to-animal variability observed. This points to the need for improvements in the design of such ECM-based biomaterials targeting the musculoskeletal system. Strategies

25

worthy of investigation include actively directing orientation of cell-deposited tissue by incorporating scaffolds with anisotropic microarchitecture [67,68] and functionalization of the scaffolds with growth factors known to play major roles in supporting hyaline cartilage formation.

5. Conclusion

Taken together, these results demonstrate the value of using tissue-specific ECM to support regeneration of complex tissues such as the osteochondral unit. Biological scaffolds derived from the ECM of small intestinal submucosa (SIS) and other tissues have paved the way for clinical application, with widespread success achieved in several reconstructive surgical-procedures such as skin replacement, vascular grafts and skeletal muscle regeneration [69]. We propose that the use of layered, tissue-specific ECM derived scaffolds, designed with the end application in mind, would build upon this early success and lead to the successful, long-term repair of complex tissues.

Data availability

The authors declare that all data supporting the findings of this study are available within the paper and its Supplementary Information.

Competing interests

The authors have no competing interests to declare.

Acknowledgements

References

[1]   T.W. Gilbert, T.L. Sellaro, S.F. Badylak, Decellularization of tissues and organs, Biomaterials. 27 (2006) 3675–3683. doi:10.1016/j.biomaterials.2006.02.014.

[2]   K.E.M. Benders, P.R. van Weeren, S.F. Badylak, D.B.F. Saris, W.J.A. Dhert, J. Malda, Extracellular matrix scaffolds for cartilage and bone regeneration, Trends Biotechnol. 31 (2013) 169–176. doi:10.1016/j.tibtech.2012.12.004.

[3]   S.F. Badylak, Xenogeneic extracellular matrix as a scaffold for tissue reconstruction, Transpl. Immunol. 12 (2004) 367–377. doi:10.1016/j.trim.2003.12.016.

[4]   C. Frantz, K.M. Stewart, V.M. Weaver, The extracellular matrix at a glance, J. Cell Sci. 123 (2010) 4195–4200. doi:10.1242/jcs.023820.

[5]   B.N. Brown, S.F. Badylak, Extracellular Matrix as an Inductive Scaffold for

Functional Tissue Reconstruction, Transl. Regen. Med. to Clin. 163 (2015) 11–29. doi:10.1016/B978-0-12-800548-4.00002-4.

[6]   J.L. Dziki, L. Huleihel, M.E. Scarritt, S.F. Badylak, Extracellular Matrix Bioscaffolds as Immunomodulatory Biomaterials, Tissue Eng. Part A. 23 (2017) 1152–1159. doi:10.1089/ten.tea.2016.0538.

[7]   L. Huleihel, J.L. Dziki, J.G. Bartolacci, T. Rausch, M.E. Scarritt, M.C. Cramer, T. Vorobyov, S.T. LoPresti, I.T. Swineheart, L.J. White, B.N. Brown, S.F. Badylak, Macrophage phenotype in response to ECM bioscaffolds, Semin. Immunol. 29 (2017) 2–13. doi:10.1016/j.smim.2017.04.004.

[8]   S.F. Badylak, The extracellular matrix as a biologic scaffold material, Biomaterials. 28 (2007) 3587–93. doi:10.1016/j.biomaterials.2007.04.043.

[9]   H. V Almeida, G.M. Cunniffe, T. Vinardell, C.T. Buckley, F.J. O'Brien, D.J. Kelly, Coupling freshly isolated CD44(+) infrapatellar fat pad-derived stromal cells with a TGF-β3 eluting cartilage ECM-derived scaffold as a single-stage strategy for promoting chondrogenesis, Adv. Healthc. Mater. 4 (2015) 1043–53. doi:10.1002/adhm.201400687.

[10] K. Shimomura, B.B. Rothrauff, R.S. Tuan, Region-Specific Effect of the Decellularized Meniscus Extracellular Matrix on Mesenchymal Stem Cell–Based Meniscus Tissue Engineering, Am. J. Sports Med. 45 (2017) 604–611. doi:10.1177/0363546516674184.

[11] G.M. Cunniffe, P.J. Díaz-Payno, J.S. Ramey, O.R. Mahon, A. Dunne, E.M. Thompson, F.J. O'Brien, D.J. Kelly, Growth plate extracellular matrix-derived scaffolds for large bone defect healing, Eur. Cell. Mater. 33 (2017) 130–142.

doi:10.22203/eCM.v033a10.

[12] F. Gao, Z. Xu, Q. Liang, B. Liu, H. Li, Y. Wu, Y. Zhang, Z. Lin, M. Wu, C. Ruan, W. Liu, Direct 3D Printing of High Strength Biohybrid Gradient Hydrogel Scaffolds for Efficient Repair of Osteochondral Defect, Adv. Funct. Mater. 28 (2018) 1706644. doi:10.1002/adfm.201706644.

[13] Y. Wu, S. Zhu, C. Wu, P. Lu, C. Hu, S. Xiong, J. Chang, B.C. Heng, Y. Xiao, H.W. Ouyang, A Bi-Lineage Conducive Scaffold for Osteochondral Defect Regeneration, Adv. Funct. Mater. 24 (2014) 4473–4483. doi:10.1002/adfm.201304304.

[14] T.J. Levingstone, A. Ramesh, R.T. Brady, P.A.J. Brama, C. Kearney, J.P. Gleeson, F.J. O'Brien, Cell-free multi-layered collagen-based scaffolds demonstrate layer specific regeneration of functional osteochondral tissue in caprine joints, Biomaterials. 87 (2016) 69–81. doi:10.1016/j.biomaterials.2016.02.006.

[15] S.N. Dehghani, A.S. Bigham, S. Torabi Nezhad, Z. Shafiei, Effect of bovine fetal growth plate as a new xenograft in experimental bone defect healing: radiological, histopathological and biomechanical evaluation, Cell Tissue Bank. 9 (2008) 91–99. doi:10.1007/s10561-008-9062-7.

[16] A.S. Bigham, S.N. Dehghani, Z. Shafiei, S.T. Nezhad, Experimental bone defect healing with xenogenic demineralized bone matrix and bovine fetal growth plate as a new xenograft: radiological, histopathological and biomechanical evaluation, Cell Tissue Bank. 10 (2009) 33–41. doi:10.1007/s10561-008-9107-y.

[17] A. Bigham-Sadegh, I. Karimi, A. Oryan, E. Mahmoudi, Z. Shafiei-Sarvestani, Spinal fusion with demineralized calf fetal growth plate as novel biomaterial in rat model: a preliminary study, Int. J. Spine Surg. 8 (2014) 5–5. doi:10.14444/1005.

[18]   H. V. Almeida, R. Eswaramoorthy, G.M. Cunniffe, C.T. Buckley, F.J. O'Brien, D.J.
       Kelly, Fibrin hydrogels functionalized with cartilage extracellular matrix and
       incorporating freshly isolated stromal cells as an injectable for cartilage regeneration,
       Acta Biomater. 36 (2016) 55–62. doi:10.1016/j.actbio.2016.03.008.

[19]   Z. Yang, Y. Shi, X. Wei, J. He, S. Yang, G. Dickson, J. Tang, J. Xiang, C. Song, G. Li,
       Fabrication and repair of cartilage defects with a novel acellular cartilage matrix
       scaffold, Tissue Eng. Part C Methods. 16 (2010) 865–76.
       doi:10.1089/ten.TEC.2009.0444.

[20]   H. V. Almeida, Y. Liu, G.M. Cunniffe, K.J. Mulhall, A. Matsiko, C.T. Buckley, F.J.
       O'Brien, D.J. Kelly, Controlled release of transforming growth factor-β3 from
       cartilage-extra-cellular-matrix-derived scaffolds to promote chondrogenesis of human-
       joint-tissue-derived stem cells, Acta Biomater. 10 (2014) 4400–9.
       doi:10.1016/j.actbio.2014.05.030.

[21]   X. Jiang, M. Ye, X. Jiang, G. Liu, S. Feng, L. Cui, H. Zou, Method Development of
       Efficient Protein Extraction in Bone Tissue for Proteome Analysis research articles, J.
       Proteome Res. 6 (2007) 2287–2294.

[22]   T. Zhou, C. Li, W. Zhao, X. Wang, F. Wang, J. Sha, MaxReport: An Enhanced
       Proteomic Result Reporting Tool for MaxQuant., PLoS One. 11 (2016) e0152067.
       doi:10.1371/journal.pone.0152067.

[23]   S. Tyanova, T. Temu, J. Cox, The MaxQuant computational platform for mass
       spectrometry-based shotgun proteomics., Nat. Protoc. 11 (2016) 2301–2319.
       doi:10.1038/nprot.2016.136.

[24]   J. Cox, I. Matic, M. Hilger, N. Nagaraj, M. Selbach, J. V Olsen, M. Mann, A practical

guide to the MaxQuant computational platform for SILAC-based quantitative

proteomics., Nat. Protoc. 4 (2009) 698–705. doi:10.1038/nprot.2009.36.

[25] S. Tyanova, T. Temu, P. Sinitcyn, A. Carlson, M.Y. Hein, T. Geiger, M. Mann, J. Cox,

The Perseus computational platform for comprehensive analysis of (prote)omics data,

Nat. Methods. 13 (2016) 731–740. doi:10.1038/nmeth.3901.

[26] A. Naba, K.R. Clauser, H. Ding, C.A. Whittaker, S.A. Carr, R.O. Hynes, The

extracellular matrix: Tools and insights for the "omics" era, Matrix Biol. 49 (2016)

10–24. doi:10.1016/j.matbio.2015.06.003.

[27] N.Y. Ignat'eva, N.A. Danilov, S. V. Averkiev, M. V. Obrezkova, V. V. Lunin, E.N.

Sobol', Determination of hydroxyproline in tissues and the evaluation of the collagen

content of the tissues, J. Anal. Chem. 62 (2007) 51–57.

doi:10.1134/S106193480701011X.

[28] P. Mainil-Varlet, B. Van Damme, D. Nesic, G. Knutsen, R. Kandel, S. Roberts, A new

histology scoring system for the assessment of the quality of human cartilage repair:

ICRS II, Am. J. Sports Med. 38 (2010) 880–890. doi:10.1177/0363546509359068.

[29] N. Reznikov, R. Almany-Magal, R. Shahar, S. Weiner, Three-dimensional imaging of

collagen fibril organization in rat circumferential lamellar bone using a dual beam

electron microscope reveals ordered and disordered sub-lamellar structures, Bone. 52

(2013) 676–683. doi:10.1016/j.bone.2012.10.034.

[30] J. Fukushi, I.T. Makagiansar, W.B. Stallcup, NG2 proteoglycan promotes endothelial

cell motility and angiogenesis via engagement of galectin-3 and alpha3beta1 integrin.,

Mol. Biol. Cell. 15 (2004) 3580–90. doi:10.1091/mbc.E04-03-0236.

[31] U. Ozerdem, W.B. Stallcup, Pathological angiogenesis is reduced by targeting

pericytes via the NG2 proteoglycan, Angiogenesis. 7 (2004) 269–276. doi:10.1007/s10456-004-4182-6.

[32]   T. Kadomatsu, M. Endo, K. Miyata, Y. Oike, Diverse roles of ANGPTL2 in physiology and pathophysiology, Trends Endocrinol. Metab. 25 (2014) 245–254. doi:10.1016/j.tem.2014.03.012.

[33]   Y. Kubota, Unveiling Angptl2, a rising HSC expander, Blood. 124 (2014) 833–834. doi:10.1182/blood-2014-06-581629.

[34]   R. Yue, B. Shen, S.J. Morrison, Clec11a/osteolectin is an osteogenic growth factor that promotes the maintenance of the adult skeleton, Elife. 5 (2016) 27. doi:10.7554/eLife.18782.

[35]   M. Inada, Y. Wang, M.H. Byrne, M.U. Rahman, C. Miyaura, C. Lopez-Otin, S.M. Krane, Critical roles for collagenase-3 (Mmp13) in development of growth plate cartilage and in endochondral ossification, Proc. Natl. Acad. Sci. 101 (2004) 17192–17197. doi:10.1073/pnas.0407788101.

[36]   D. Stickens, Altered endochondral bone development in matrix metalloproteinase 13-deficient mice, Development. 131 (2004) 5883–5895. doi:10.1242/dev.01461.

[37]   A. Cmoch, A. Strzelecka-Kiliszek, M. Palczewska, P. Groves, S. Pikula, S100A4 and S100A10 proteins as regulators of matrix vesicle mediated mineralization of osteoblast-like cells, Bone. 50 (2012) S69–S70. doi:10.1016/j.bone.2012.02.196.

[38]   R. Donato, B. R. Cannon, G. Sorci, F. Riuzzi, K. Hsu, D. J. Weber, C. L. Geczy, Functions of S100 Proteins, Curr. Mol. Med. 13 (2013) 24–57. doi:10.2174/156652413804486214.

[39] J.C.H. Leijten, J. Emons, C. Sticht, S. Van Gool, E. Decker, A. Uitterlinden, G. Rappold, A. Hofman, F. Rivadeneira, S. Scherjon, J.M. Wit, J. Van Meurs, C.A. Van Blitterswijk, M. Karperien, Gremlin 1, frizzled-related protein, and dkk-1 are key regulators of human articular cartilage homeostasis, Arthritis Rheum. 64 (2012) 3302–3312. doi:10.1002/art.34535.

[40] S. Ohno, T. Doi, S. Tsutsumi, Y. Okada, K. Yoneno, Y. Kato, K. Tanne, RGD-CAP (βig-h3) is expressed in precartilage condensation and in prehypertrophic chondrocytes during cartilage development, Biochim. Biophys. Acta - Gen. Subj. 1572 (2002) 114–122. doi:10.1016/S0304-4165(02)00286-6.

[41] S. Ohno, M. Noshiro, S. Makihira, T. Kawamoto, M. Shen, W. Yan, Y. Kawashima-Ohya, K. Fujimoto, K. Tanne, Y. Kato, RGD-CAP (βig-h3) enhances the spreading of chondrocytes and fibroblasts via integrin α1β1, Biochim. Biophys. Acta - Mol. Cell Res. 1451 (1999) 196–205. doi:10.1016/S0167-4889(99)00093-2.

[42] M.S. Bendre, D.C. Montague, T. Peery, N.S. Akel, D. Gaddy, L.J. Suva, Interleukin-8 stimulation of osteoclastogenesis and bone resorption is a mechanism for the increased osteolysis of metastatic bone disease, Bone. 33 (2003) 28–37. doi:10.1016/S8756-3282(03)00086-3.

[43] P. Kopesky, K. Tiedemann, D. Alkekhia, C. Zechner, B. Millard, B. Schoeberl, S. V. Komarova, Autocrine signaling is a key regulatory element during osteoclastogenesis, Biol. Open. 3 (2014) 767–776. doi:10.1242/bio.20148128.

[44] A.M. Handorf, W.-J. Li, Fibroblast Growth Factor-2 Primes Human Mesenchymal Stem Cells for Enhanced Chondrogenesis, PLoS One. 6 (2011) e22887. doi:10.1371/journal.pone.0022887.

[45]   E. Kon, G. Filardo, F. Perdisa, G. Venieri, M. Marcacci, Clinical results of

multilayered biomaterials for osteochondral regeneration, J. Exp. Orthop. 1 (2014) 10.

doi:10.1186/s40634-014-0010-0.

[46]   J.I. Fukushi, M. Inatani, Y. Yamaguchi, W.B. Stallcup, Expression of NG2

proteoglycan during endochondral and intramembranous ossification, Dev. Dyn. 228

(2003) 143–148. doi:10.1002/dvdy.10359.

[47]   W. De Spiegelaere, P. Cornillie, C. Casteleyn, C. Burvenich, W. Van den Broeck,

Detection of Hypoxia Inducible Factors and Angiogenic Growth Factors during Foetal

Endochondral and Intramembranous Ossification, J. Vet. Med. Ser. C Anat. Histol.

Embryol. 39 (2010) 376–384. doi:10.1111/j.1439-0264.2010.01005.x.

[48]   T.H. Vu, J.M. Shipley, G. Bergers, J.E. Berger, J.A. Helms, D. Hanahan, S.D. Shapiro,

R.M. Senior, Z. Werb, MMP-9/gelatinase B is a key regulator of growth plate

angiogenesis and apoptosis of hypetrophic chondrocytes, Cell. 93 (1998) 411–422.

doi:10.1016/S0092-8674(00)81169-1.

[49]   H. Nagai, M. Aoki, Inhibition of growth plate angiogenesis and endochondral

ossification with diminished expression of MMP-13 in hypertrophic chondrocytes in

FGF-2-treated rats, J. Bone Miner. Metab. 20 (2002) 142–147.

doi:10.1007/s007740200020.

[50]   L.L. Lourido, V. Calamia, J.J. Mateos, P. Fernandez-Puente, J. Fernandez-Tajes, F.J.

Blanco, C. Ruiz-Romero, P. Fernández-Puente, J. Fernández-Tajes, F.J. Blanco, C.

Ruiz-Romero, Quantitative proteomic profiling of human articular cartilage

degradation in osteoarthritis., J. Proteome Res. 13 (2014) 6096–106.

doi:10.1021/pr501024p.

34

[51]   H.C. Anderson, P.T. Hodges, X.M. Aguilera, L. Missana, P.E. Moylan, Bone

Morphogenetic Protein (BMP) Localization in Developing Human and Rat Growth

Plate, Metaphysis, Epiphysis, and Articular Cartilage, J. Histochem. Cytochem. 48

(2000) 1493–1502. doi:10.1177/002215540004801106.

[52]   E. Tchetina, F. Mwale, a R. Poole, Distinct phases of coordinated early and late gene

expression in growth plate chondrocytes in relationship to cell proliferation, matrix

assembly, remodeling, and cell differentiation., J. Bone Miner. Res. 18 (2003) 844–51.

doi:10.1359/jbmr.2003.18.5.844.

[53]   A.I. Alford, K.M. Kozloff, K.D. Hankenson, Extracellular matrix networks in bone

remodeling, Int. J. Biochem. Cell Biol. 65 (2015) 20–31.

doi:10.1016/j.biocel.2015.05.008.

[54]   M. Tamaddon, M. Burrows, S.A. Ferreira, F. Dazzi, J.F. Apperley, A. Bradshaw, D.D.

Brand, J. Czernuszka, E. Gentleman, Monomeric, porous type II collagen scaffolds

promote chondrogenic differentiation of human bone marrow mesenchymal stem cells

in vitro, Sci. Rep. 7 (2017) 1–10. doi:10.1038/srep43519.

[55]   M.K. Khokha, D. Hsu, L.J. Brunet, M.S. Dionne, R.M. Harland, Gremlin is the BMP

antagonist required for maintenance of Shh and Fgf signals during limb patterning,

Nat. Genet. 34 (2003) 303–307. doi:10.1038/ng1178.

[56]   D.L. Worthley, M. Churchill, J.T. Compton, Y. Tailor, M. Rao, Y. Si, D. Levin, M.G.

Schwartz, A. Uygur, Y. Hayakawa, S. Gross, B.W. Renz, W. Setlik, A.N. Martinez, X.

Chen, S. Nizami, H.G. Lee, H.P. Kang, J.-M. Caldwell, S. Asfaha, C.B. Westphalen,

T. Graham, G. Jin, K. Nagar, H. Wang, M.A. Kheirbek, A. Kolhe, J. Carpenter, M.

Glaire, A. Nair, S. Renders, N. Manieri, S. Muthupalani, J.G. Fox, M. Reichert, A.S.

Giraud, R.F. Schwabe, J.-P. Pradere, K. Walton, A. Prakash, D. Gumucio, A.K. Rustgi, T.S. Stappenbeck, R.A. Friedman, M.D. Gershon, P. Sims, T. Grikscheit, F.Y. Lee, G. Karsenty, S. Mukherjee, T.C. Wang, Gremlin 1 identifies a skeletal stem cell with bone, cartilage and reticular stromal potential, Cell. 160 (2015) 269–84. doi:10.1016/j.cell.2014.11.042.

[57]   N. Thapa, B.H. Lee, I.S. Kim, TGFBIp/βig-h3 protein: A versatile matrix molecule induced by TGF-β, Int. J. Biochem. Cell Biol. 39 (2007) 2183–2194. doi:10.1016/j.biocel.2007.06.004.

[58]   P. Önnerfjord, A. Khabut, F.P. Reinholt, O. Svensson, D. Heinegård, Quantitative proteomic analysis of eight cartilaginous tissues reveals characteristic differences as well as similarities between subgroups, J. Biol. Chem. 287 (2012) 18913–24. doi:10.1074/jbc.M111.298968.

[59]   M.F. Hsueh, A. Khabut, S. Kjellström, P. Önnerfjord, V.B. Kraus, Elucidating the Molecular Composition of Cartilage by Proteomics, J. Proteome Res. 15 (2016) 374–388. doi:10.1021/acs.jproteome.5b00946.

[60]   A. Naba, O.M.T. Pearce, A. Del Rosario, D. Ma, H. Ding, V. Rajeeve, P.R. Cutillas, F.R. Balkwill, R.O. Hynes, Characterization of the Extracellular Matrix of Normal and Diseased Tissues Using Proteomics, J. Proteome Res. 16 (2017) 3083–3091. doi:10.1021/acs.jproteome.7b00191.

[61]   M. Berruto, M. Delcogliano, F. de Caro, G. Carimati, F. Uboldi, P. Ferrua, G. Ziveri, C.F. De Biase, Treatment of Large Knee Osteochondral Lesions With a Biomimetic Scaffold: Results of a Multicenter Study of 49 Patients at 2-Year Follow-up, Am. J. Sports Med. 42 (2014) 1607–17. doi:10.1177/0363546514530292.

[62]   E. Kon, M. Delcogliano, G. Filardo, M. Fini, G. Giavaresi, S. Francioli, I. Martin, D. Pressato, E. Arcangeli, R. Quarto, M. Sandri, M. Marcacci, Orderly osteochondral regeneration in a sheep model using a novel nano-composite multilayered biomaterial, J. Orthop. Res. 28 (2010) 116–124. doi:10.1002/jor.20958.

[63]   G. Calabrese, R. Giuffrida, S. Forte, L. Salvatorelli, C. Fabbi, E. Figallo, M. Gulisano, R. Parenti, G. Magro, C. Colarossi, L. Memeo, R. Gulino, Bone augmentation after ectopic implantation of a cell-free collagen-hydroxyapatite scaffold in the mouse, Sci. Rep. 6 (2016) 1–10. doi:10.1038/srep36399.

[64]   A.R. Gannon, T. Nagel, A.P. Bell, N.C. Avery, D.J. Kelly, Postnatal changes to the mechanical properties of articular cartilage are driven by the evolution of its Collagen network, Eur. Cells Mater. 29 (2015) 105–123. doi:vol029a09 [pii].

[65]   H.M. Kronenberg, H.M. Kronenberg, Developmental regulation of the growth plate, Nature. 423 (2003) 332–6. doi:10.1038/nature01657.

[66]   P.M. Crapo, T.W. Gilbert, S.F. Badylak, An overview of tissue and whole organ decellularization processes, Biomaterials. 32 (2011) 3233–43. doi:10.1016/j.biomaterials.2011.01.057.

[67]   E.L.W. De Mulder, G. Hannink, T.H. Van Kuppevelt, W.F. Daamen, P. Buma, Similar Hyaline-Like Cartilage Repair of Osteochondral and Anisotropic Collagen Scaffolds, Tissue Eng. Part A. 20 (2014) 635–645. doi:10.1089/ten.tea.2013.0083.

[68]   H. V. Almeida, B.N. Sathy, I. Dudurych, C.T. Buckley, F.J. O'Brien, D.J. Kelly, Anisotropic Shape-Memory Alginate Scaffolds Functionalized with Either Type I or Type II Collagen for Cartilage Tissue Engineering, Tissue Eng. Part A. 23 (2017) 55–68. doi:10.1089/ten.tea.2016.0055.

[69] B. Andrée, A. Bär, A. Haverich, A. Hilfiker, Small Intestinal Submucosa Segments as Matrix for Tissue Engineering: Review, Tissue Eng. Part B Rev. 19 (2013) 279–291. doi:10.1089/ten.teb.2012.0583.